DALTON
FULL PAPER

Electronic communication between carbon chain bridged metals: a theoretical approach. Even Chains †

Paola Belanzoni,[a] Nazzareno Re,[a] Antonio Sgamellotti *,[a] and Carlo Floriani [b]

[a] *Dipartimento di Chimica and Centro di Studio CNR per il Calcolo Intensivo in Scienze Molecolari, Università di Perugia, via Elce di Sotto 8, I-06123 Perugia, Italy*
[b] *Institut de Chimie Minérale et Analytique, BCH Université de Lausanne, CH-1015, Lausanne, Switzerland*

A theoretical investigation (DFT) allowed us to single out the most appropriate valence structure for the [M–C_x–M] unit in a variety of model compounds [{$Cp(CO)_2M$}$_2$(μ-C_x)] (M = Cr, Mn or Fe; x = 2–8) and to foresee it on the basis of the molecular parameters, such as (i) the chain length, (ii) the nature of the metal and its oxidation state, (iii) the d^n configuration and the metal co-ordination number. The valence structure of the [M–C_x–M] unit is diagnostic of the metal-to-metal communication. A simple electron-counting scheme has been developed to predict the valence structure, based on the d^n configuration of the ML_m fragments and the number of p_π electrons of the linear C_x unit.

Several organometallic complexes in which two transition-metal atoms are bridged by linear unsaturated carbon chains, $L_mMC_xML_m$, have attracted much interest.[1–5] Although the most common examples are those with x = 2 [6–18] higher homologues have been recently synthesized with x = 4–20.[19–39] Such complexes constitute a first step in the synthesis of elemental carbon fragments or allotropes stabilized by transition-metal complexes.[3] Moreover, they exhibit potentially useful material properties and have considerable theoretical importance. On increasing the length of the C_x chain, analogies with polyacetylene and the possibility of long-range interactions between the two metals become apparent and make these systems interesting examples of one-dimensional molecular wires.

All of the synthesized C_x bridged complexes have a number of common features: (i) the metal fragments spanning the bridge are constituted by mid to late transition metals in rather low oxidation state with π-acceptor ligands; (ii) particularly widespread are fragments like CpMLL′ (L,L′ = CO, NO or PR_3; M = Mn, Re or Fe) with co-ordination number five; (iii) the metal configurations of these fragments are d^6 and d^7 with very few d^5 exceptions.

Among the C_x bridged dinuclear complexes which have been synthesized, structural and synthetic reasons suggest that one can distinguish between compounds with an even number of carbon atoms (C_{2x}) and those with an odd number of carbon atoms (C_{2x+1}). This difference is already evident in the simple HC_xH series (known only for even x)[40] and arises from the different nature of the ground states for compounds with an even and an odd number of carbon atoms; a stable closed shell singlet in the former case and an unstable open shell triplet in the latter case.[41] Bridged dinuclear compounds with an even C_x bridge are by far more common. Several four-carbon bridged complexes are known with structures similar to those of butadiyne, described as alternating single and triple bonds.[19–27,29,32,33] Typical examples are [{Cp*Re$(PPh_3)(NO)$}$_2$-(μ-C_4)] **1** [19,20] and [{Cp*Fe(dppe)}$_2$(μ-C_4)] **2** [32,33] which have been isolated for different oxidation states of the metal. Depending on the d^n configuration, the C_4 chain displays either a polyynic (reduced) form or a cumulenic (oxidized) structure (Scheme 1) as is the case for the C_6 and C_8 bridges in complexes [{Cp*Re-$(PPh_3)(NO)$}$_2$(μ-C_6)] **3** and [{Cp*Re$(PPh_3)(NO)$}$_2$(μ-C_8)] **4** [28]

† *Non-SI unit employed*: eV ≈ 1.60 × 10^{-19} J.

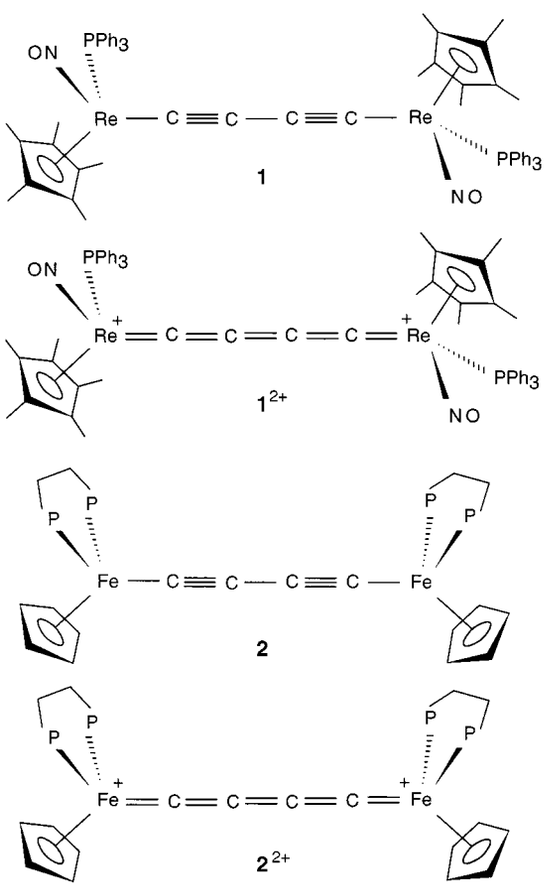

Scheme 1

which undergo two reversible one-electron oxidations (see Scheme 2).

A recent synthetic and electrochemical study by Gladysz and co-workers [30,31] on [{Cp*Re$(PPh_3)(NO)$}$_2$(μ-C_x)] compounds containing longer chains (x = 12–20) led to a relationship between the C_x chain length and the metal-to-metal communication as a function of the chain length.

The communication between the two metals can be expressed by the three valence structures (**A**, **B** and **C** in Scheme 3) related

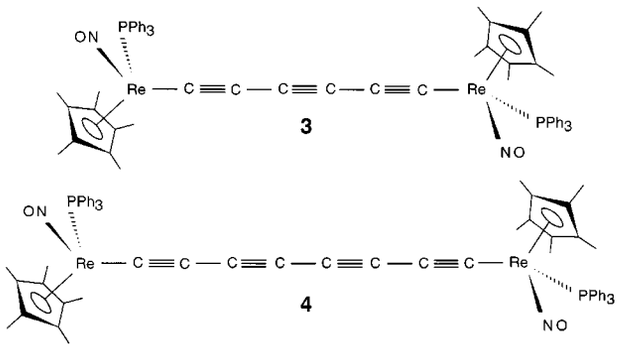

Scheme 2

$$[M(-C\equiv C-)_{\frac{x}{2}}M]^{z+} \overset{-2e^-}{\rightleftharpoons} [M(=C=C=)_{\frac{x}{2}}M]^{(z+2)+} \overset{-2e^-}{\rightleftharpoons} [M(\equiv C-C\equiv)_{\frac{x}{2}}M]^{(z+4)+}$$

A **B** **C**

Scheme 3

to the C_x (x even) chains. The three valence structures are formally related by two-electron oxidations as shown in Scheme 3.[27]

In the same context, we should mention that an important complementary series of bimetallic chain bridged complexes is $[\{Cp^*Fe(dppe)\}_2(\mu\text{-}C_x)]$, $x = 2$–8, developed by Lapinte and co-workers.[32–34]

Very few compounds have been synthesized with an odd number of carbons in the C_x bridge[35–39] containing C_3 and C_5 chains, only one three-carbon bridged complex has been structurally characterized, $[\{Cp^*Re(PPh_3)(NO)\}(\mu\text{-}C_3)\{CpMn(CO)_2\}]^+$.[37] For each of these C_3 and C_5 chains we can draw two possible valence structures (Scheme 4) and all the spectroscopic and structural informations indicate that the resonance cumulenic forms **6** and **7** dominate over the polyynic ones, **5** and **8**.[37,38]

Few theoretical investigations have been performed on C_2 bridged dinuclear complexes,[6,7,10] and only one has been carried out on longer carbon bridges, *i.e.* a $[\{Cp^*Re(PPh_3)(NO)\}_2(\mu\text{-}C_4)]$ species.[29] In two recent papers,[42,43] we carried out DFT calculations on a wide class of C_2 dinuclear complexes of transition metals giving a qualitative interpretation of the bonding that occurs between the two metal atoms and the bridging C_2 ligand in terms of a simple molecular orbital scheme for four-center M–C–C–M π and δ interactions and developing a simple qualitative model which enables one to forecast the valence bond structure on the basis of the characteristics of the two transition-metal fragments, ML_m.

Herein, we address a general theoretical study on the even C_x bridged complexes mentioned above. A study of odd chain complexes will be presented in a forthcoming paper. We have performed LCAO density functional calculations on the $[\{CpM(CO)_2\}_2(\mu\text{-}C_x)]$ (M = Cr, Mn or Fe; $x = 4$ or 6 and $x = 2$ or 8 only for M = Fe) series (see Fig. 1) as models of the even C_x bridged complexes where the metal is bound to π-acceptor ligands in a pseudo-octahedral co-ordination. The move from Cr to Fe allowed us to study the dependence on the nature of the metal, its oxidation state and d configurations.

Some model compounds have been chosen as close as possible to the experimental ones in order to compare selected excitation and ionization energies and eventually to determine a correlation with the chain length. Such calculations have allowed us: (i) to clarify the electronic structure of these complexes; (ii) to point out the factors which determine the geometric structure, *i.e.* cumulenic *vs*. alternating single and triple bonds; (iii) to investigate the effect of lengthening the carbon chain; (iv) to study the electron delocalization across the wire-like C_x bridges and the metal–metal interaction between them.

Among the main results, we have found optimized structures consistent with the experimentally characterized geometries,

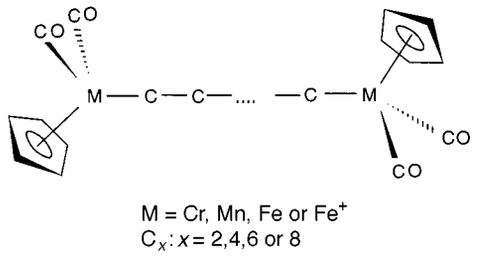

Fig. 1 Geometrical structures of the considered model complexes

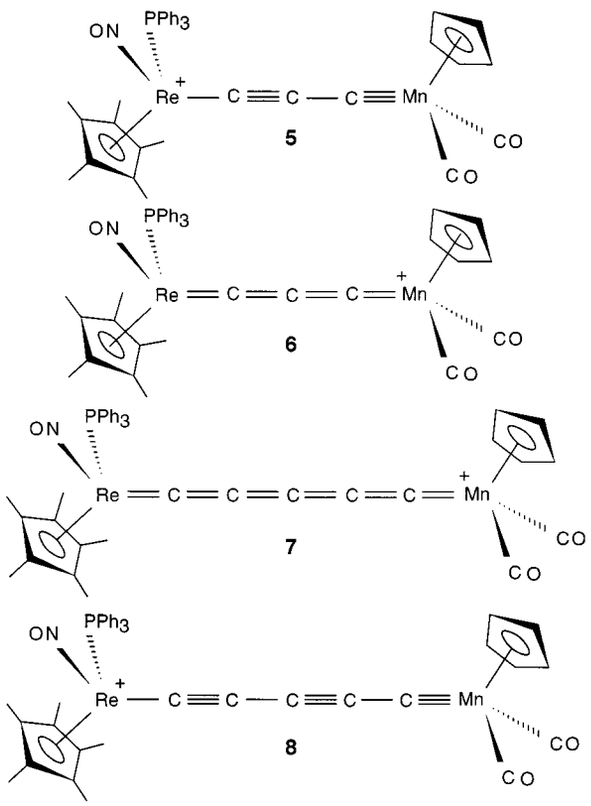

Scheme 4

giving a rationale for their occurrence in terms of the electron count on the metal fragments.

Computational and Methodological Details

The calculations reported in this paper are based on the ADF (Amsterdam density functional) program package described elsewhere.[44–46] Its main characteristics are the use of a density fitting procedure to obtain accurate Coulomb and exchange potentials in each SCF cycle, the accurate and efficient numerical integration of the effective one-electron Hamiltonian matrix elements and the possibility to freeze core orbitals. The molecular orbitals were expanded in an uncontracted double-ζ STO basis set for all atoms with the exception of the transition-metal orbitals for which we used a double-ζ STO basis set for 3s and 3p and a triple-ζ STO basis set for 3d and 4s. As polarization functions, one 4p, one 3d and one 2p STO were used for transition metals, O and C, and H, respectively. The cores (Cr, Mn, Fe: 1s–2p; C, O: 1s) have been kept frozen.

The LDA exchange correlation potential and energy were used, together with the Vosko–Wilk–Nusair parametrization[47] for homogeneous electron–gas correlation, including Becke's non-local correction[48] to the local exchange expression and Perdew's non-local correction[49] to the local expression of correlation energy (NLDA). Molecular structures were optimized by the NLDA method in C_{2h} (or C_s) symmetry.

To study the electronic structure of the mixed-valence $[\{Cp(CO)_2Fe\}_2(\mu\text{-}C_x)]^+$ ($x = 4$–8) complexes we used the broken symmetry spin unrestricted approach. This technique, developed by Noodleman and Norman,[50] avoids the problem of a constrained equal amplitude of molecular orbitals over the two metal centres and allows the unpaired electron to localize on one center if such an arrangement is energetically favourable. To reach this goal, we removed the inversion center through the bridging chain lowering the symmetry from the C_{2h} geometrical symmetry to C_s.

In order to analyze the $[Cp(CO)_2M]$–C_x interaction energies, we use a method that is an extension of the well known decomposition scheme of Morokuma.[51] The bonding energy is decomposed into a number of terms. The first term, ΔE^o, which is called the steric repulsion, consists of two components. The first is the electrostatic interaction ΔE_{elstat} of the nuclear charges and unmodified electronic charge density of one fragment with those of the other fragment, both fragments being at their final positions. The second component is the so-called Pauli repulsion ΔE_{Pauli}, which is essentially due to the antisymmetry requirement on the total wavefunction. In addition to the steric repulsion term ΔE^o there are the attractive orbital interactions which give rise to an energy lowering, the orbital interaction energy ΔE_{oi}. This term may be broken up into contributions from the orbital interactions within the various irreducible representations Γ of the overall symmetry group of the system, according to the decomposition scheme proposed by Ziegler and Rauk.[52]

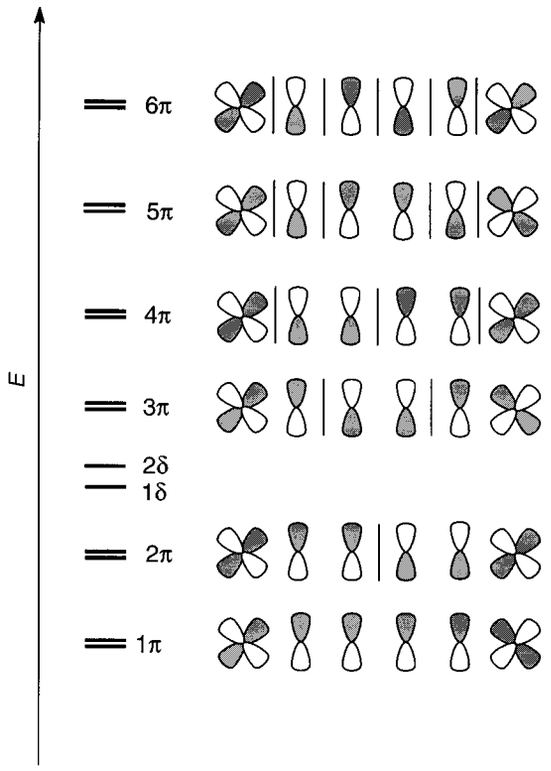

Scheme 5

Results and Discussion

A qualitative Hückel-type model

We propose here a simple molecular orbital scheme for $(x + 2)$-center M–C_x–M π and δ interactions which is an extension of that proposed to explain bonding in dinitrogen-bridged[53] and μ-C_2 bridged transition-metal dimers and employed to interpret the results of some theoretical calculations on these complexes.[42,54–57] The assumptions on which this model is based will be justified in the next paragraph on the basis of the accurate DFT calculations. In such a model, we assume that the energy order of the bridging orbitals, classified on the basis of their symmetry with respect to the M–C_x–M axis (assumed to be the z axis), is $\sigma \ll \pi \leq \delta \leqslant \delta^* \leqslant \pi^* \ll \sigma^*$. This implies that the metal d_{z^2} orbitals strongly interact with the sp hybrids of the terminal carbon atoms forming two M–C σ bonds, while the other carbon sp hybrids form $(x - 1)$ C–C σ bond MOs at an even lower energy. The uppermost frontier orbitals involved in the bonding of the C_x bridge are therefore those originating from the interactions of the carbon π with the metal d_π orbitals and can be built within a simple Hückel-type approach. Assuming comparable energies for the C p_π and the M d_π orbitals, the π-system is constituted by the $(x + 2)$-center molecular orbitals qualitatively illustrated in Scheme 5 for $x = 4$.

Two sets of these $(x + 2)$-center molecular orbitals are actually obtained by linear combinations of M d_{xz}, C p_x or M d_{yz}, C p_y orbitals. Depending on the overall molecular symmetry, the energy diagram is therefore made up by $(x + 2)$ doubly degenerate levels (D_{2d} symmetry or higher) or by $(x + 2)$ closely spaced couples of levels (C_{2h} symmetry or lower) whose energies increase with increasing nodal planes and which are designated as 1π–$(x + 2)$π. The overall scheme is completed by the orbitals of δ symmetry built by the bonding and antibonding combinations of the d_{xy}, and eventually also the $d_{x^2-y^2}$, orbitals depending on the co-ordination geometry of the L_mM fragment. These orbitals do not interact with any C_x orbital and give no contribution to the bonding; they should lie between 1π and $(x + 2)$π and will be designated as 1δ–4δ. The nature of the metals and of the ligands and the co-ordination geometry in the metal fragments determine the energy of the metal d orbitals and, therefore, both the metal character of the 1π–$(x + 2)$π orbitals and the relative position of the 1δ–4δ levels.

If the σ M–C_x–M skeleton is regarded as mainly constant, the variation in the M–C and C–C bond character can be attributed to changes in the nature and in the occupancy of the π frontier orbitals. When the occupancy of these levels is taken into account, we found it convenient to perform the electron count by considering a neutral C_x molecule bracketed by the two metal ML_m fragments. Therefore, the d^n configuration attributed to the ML_m fragment is at least one unit higher than that attributable to the metal in the whole complex on the basis of the conventional oxidation state assignment. If each L_mM fragment has a d^n configuration, a total of $2(n - 1) + 2x$ electrons are left to occupy these π and δ frontier orbitals; $2x$ coming from the C_x unit and $n - 1$ from each metal fragment (one is employed in the M–C σ bond). A relevant difference between systems with an even bridge and those with an odd one arises when these electrons are distributed on the π orbitals.

Let us first consider an even bridging chain taking as an example a $L_mMC_4ML_m$ complex with the metal in a pseudo-octahedral co-ordination. The energy level diagram foreseen for the π–δ system of this complex is illustrated in Scheme 5. To distinguish the carbon atoms along the chain, we will use greek letters beginning from the first carbon atom on the left, *i.e.* M–C_α–C_β–C_γ–. . .–M. Note that for the pseudo-octahedral co-ordination of the metal fragment the $d_{x^2-y^2}$ levels are destabilized by σ interactions with the ligands, leaving only two δ levels at energies close to that of the 3π orbital (see Scheme 5). For metal fragments with a d^7 configuration, these orbitals should be filled with 20 electrons and the HOMO is the 4π one. The molecular geometry is mainly determined by the nodal pattern of such a HOMO which shows three nodal planes, two between each metal atom and the outer C_α and C_δ carbons, and one between the two central C_β and C_γ carbons. These nodes weaken the π bond contribution built up by the occupied 1π–3π orbitals and strongly support a polyyne-like structure **A** (see Scheme 3). For metal fragments with a d^6 configuration, like $[Mn(CO)_2Cp]$, the HOMO is only half filled so that the geometry is expected to change toward a cumulene-like structure **B**. Moreover, a triplet ground state is expected, at least if the sys-

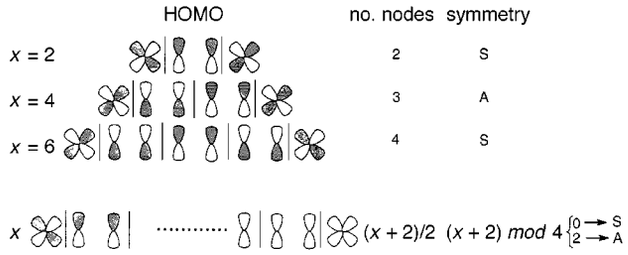

Scheme 6

tem has a high enough symmetry.[58,59] For a metal fragment with a d^5 configuration the 4π orbital is empty, the HOMO is the 3π orbital with nodal planes between C_α–C_β and C_γ–C_δ, so that a polyyne-like structure **C** is expected. Analogous arguments apply to larger even carbon chains making use of the topology of Hückel orbitals. For a $L_mMC_xML_m$ complex based on metal fragments with a d^7 configuration, the HOMO is the $(\frac{x}{2} + 2)\pi$ orbital which has $\frac{x}{2} + 1$ nodes. Taking into account that (i) this orbital is symmetric (S) or antisymmetric (A) with respect to the bisecting plane depending on the value of $(x + 2)$ *mod* 4, S if $(x + 2)$ *mod* 4 is 0, A if $(x + 2)$ *mod* 4 is 2;[58,59] (ii) the nodes must be as distributed as possible, we can predict the nodal pattern illustrated in Scheme 6. The arithmetic operation *mod* 4 stands for the subtraction from $x + 2$ of the maximum multiple of four, *e.g.* for a C_4 bridge we have $x + 2$ *mod* $4 = 6$ *mod* $4 = 2$ so that the 4π HOMO is antisymmetric, while for a C_6 bridge we have $x + 2$ *mod* $4 = 8$ *mod* $4 = 0$ so that the 5π HOMO is symmetric and so on (see Scheme 6). This pattern suggests a polyyne-like structure **A**. For a d^5 metal fragment the HOMO is the $(\frac{x}{2} + 1)\pi$ orbital which has $\frac{x}{2}$ nodes shifted by one place with respect to those of the $(\frac{x}{2} + 2)\pi$, so that a polyyne-like structure **C** is foreseen. An intermediate cumulene-like structure **B** is expected for a d^6 metal fragment for which the $(\frac{x}{2} + 2)\pi$ orbital is only half filled.

DFT calculations on the [{CpM(CO)$_2$}$_2$(μ-C$_x$)] series

The ground states and configurations of the considered complexes with C_4 and C_6 chains are reported in Table 1. For the considered complexes with an even chain, the ground state is a singlet, ^1A_g, or a triplet, ^3B_g, depending only on the metal fragment. We have found a singlet ground state for the Cr (d^5 fragment configuration) and Fe (d^7) complexes and for the Fe dicationic species (d^6) and a triplet ground state for Mn (d^6) complexes. Table 2 illustrates the optimized geometries in the [{Cp(CO)$_2$M}$_2$(μ-C$_x$)] (M = Cr, Mn or Fe; $x = 4,6$) series of complexes, including the dicationic iron species. The main geometrical parameters of the [{Cp(CO)$_2$Fe}$_2$(μ-C$_x$)] and [(CH$_3$)$_2$-(μ-C$_x$)], $x = 2$, 4, 6 or 8 species and the corresponding HOMO–LUMO gaps are compared in Table 3. The species [{Cp-(CO)$_2$Fe}$_2$(μ-C$_4$)] **9** and [{Cp(CO)$_2$Fe}$_2$(μ-C$_6$)] **10** are stable closed shell singlets and show the highest HOMO–LUMO gaps in the two [{Cp(CO)$_2$M}$_2$(μ-C$_4$)] and [{Cp(CO)$_2$M}$_2$(μ-C$_6$)] series and their MO diagrams will serve as a basis for the discussion of all other complexes. The computed valence energy levels of these latter iron dimers, labeled according to C_{2h} symmetry, are reported in Tables 4 and 5. The orbitals of main metal or C_x character are classified on the basis of their symmetry with respect to the M–C_x–M axis (the *y* axis) in σ, π, δ, σ*, π* and δ*.

The electronic interaction between the even C_x unit and the metal fragments will be discussed by considering a fragment approach in which the two [Cp(CO)$_2$M] fragments interact with a C_x species, and therefore by employing the same electron count used in the Hückel-like model. The main valence orbitals of the [Cp(CO)$_2$M] (M = Cr, Mn or Fe) fragments (C_s symmetry) are reported in Fig. 2. The frontier d orbitals split into a lower set of three t_{2g}-like orbitals, labeled as 17a′(d_{z^2}), 12a″(d_{yz}) and 18a′(d_{xy}) in the C_s point group, and a higher set of e_g-like orbitals, labeled as 19a′($d_{x^2-y^2}$) and 13a″(d_{xz}). One of the two d_δ orbitals (17a′) lies at lower energy because it is stabilized by the back bonding to the CO π*, while the other one (13a″) lies at higher energy due to the interactions with the CO 5σ. The d_π orbitals, 18a′ and 12a″, are almost degenerate and are stabilized by the back bonding to the CO π*. The 19a′ is a d_σ orbital (dsp hybrid) and is singly occupied in the iron fragment. The C_x molecules ($x = 2$, 4, 6 or 8) have been considered in the $^3\Sigma_u^+$ triplet state, corresponding to the valence state prepared to interact with the metal σ orbitals, with bond distances equal to those found in the corresponding dinuclear complexes. Their main valence orbitals are reported on the right in Figs. 3 and 4 for C_4 and C_6, respectively. In each case the singly occupied orbitals ($2\sigma_u$ and $3\sigma_g$ for C_4, and $3\sigma_u$ and $4\sigma_g$ for C_6 in $D_{\infty h}$ symmetry) correspond to the in-phase and out-of-phase combinations of the terminal carbon sp hybrids and are of the right symmetry to interact with the metal d_σ orbitals. The HOMO $1\pi_g$ for C_4, and $2\pi_u$ for C_6 correspond to the two highest orthogonal π orbitals while the LUMO $2\pi_u$ for C_4, $2\pi_g$ for C_6 correspond to the two lowest π* orbitals. Figs. 3 and 4 show the

Table 1 Metal d^n configurations, complex configurations, electronic states and energies (with respect to atoms) for the chromium, manganese, iron, monocationic and dicationic iron complexes

Complex	Metal d configuration	Complex configuration	State	Energy/eV
[{Cp(CO)$_2$Cr}$_2$(μ-C$_4$)]	d^5	$(21a_g)^2$	^1A_g	−235.51
[{Cp(CO)$_2$Mn}$_2$(μ-C$_4$)]	d^6	$(22a_g)^1(13b_g)^1$	^3B_g	−235.91
[{Cp(CO)$_2$Fe}$_2$(μ-C$_4$)]	d^7	$(22a_g)^2(13b_g)^2$	^1A_g	−234.65
[{Cp(CO)$_2$Fe}$_2$(μ-C$_4$)]$^+$	d^6/d^7	$(22a_g)^2(13b_g)^1$	^2B_g	−227.99
[{Cp(CO)$_2$Fe}$_2$(μ-C$_4$)]$^{2+}$	d^6	$(22a_g)^2(13b_g)^0$	^1A_g	−217.79
[{Cp(CO)$_2$Cr}$_2$(μ-C$_6$)]	d^5	$(23a_g)^2$	^1A_g	−251.46
[{Cp(CO)$_2$Mn}$_2$(μ-C$_6$)]	d^6	$(14a_u)^1(23b_u)^1$	^3B_g	−252.02
[{Cp(CO)$_2$Fe}$_2$(μ-C$_6$)]	d^7	$(14a_u)^2(23b_u)^2$	^1A_g	−250.75
[{Cp(CO)$_2$Fe}$_2$(μ-C$_6$)]$^+$	d^6/d^7	$(14a_u)^1(23b_u)^2$	^2B_g	−244.16
[{Cp(CO)$_2$Fe}$_2$(μ-C$_6$)]$^{2+}$	d^6	$(14a_u)^0(23b_u)^2$	^1A_g	−234.26

Table 2 Main optimized geometrical parameters of [{Cp(CO)$_2$M}$_2$-(μ-C$_x$)] complexes, M = Cr, Mn or Fe; $x = 4$ or 6

Complex	Parameter	NLDA/Å
[{Cp(CO)$_2$Cr}$_2$(μ-C$_4$)]	Cr–C (C_4)	1.746
	C_α–C_β	1.318
	C_β–C_γ	1.260
[{Cp(CO)$_2$Mn}$_2$(μ-C$_4$)]	Mn–C (C_4)	1.810
	C_α–C_β	1.273
	C_β–C_γ	1.305
[{Cp(CO)$_2$Fe}$_2$(μ-C$_4$)]	Fe–C (C_4)	1.900
	C_α–C_β	1.230
	C_β–C_γ	1.356
[{Cp(CO)$_2$Fe}$_2$(μ-C$_4$)]$^{2+}$	Fe–C (C_4)	1.787
	C_α–C_β	1.271
	C_β–C_γ	1.298
[{Cp(CO)$_2$Cr}$_2$(μ-C$_6$)]	Cr–C (C_6)	1.746
	C_α–C_β	1.319
	C_β–C_γ	1.258
	C_γ–C_δ	1.304
[{Cp(CO)$_2$Mn}$_2$(μ-C$_6$)]	Mn–C (C_6)	1.800
	C_α–C_β	1.273
	C_β–C_γ	1.296
	C_γ–C_δ	1.265
[{Cp(CO)$_2$Fe}$_2$(μ-C$_6$)]	Fe–C (C_6)	1.891
	C_α–C_β	1.233
	C_β–C_γ	1.342
	C_γ–C_δ	1.232
[{Cp(CO)$_2$Fe}$_2$(μ-C$_6$)]$^{2+}$	Fe–C (C_6)	1.786
	C_α–C_β	1.270
	C_β–C_γ	1.292
	C_γ–C_δ	1.265

orbital interaction diagrams of **9** and **10** which are representative of the behavior in the whole $[\{Cp(CO)_2M\}_2(\mu\text{-}C_x)]$ series. In all of these complexes, the orbitals describing the interaction between metal atoms and the bridging C_x, $x = 4$ or 6 moiety can be divided into four groups: (i) two low-lying orbitals describing the σ M–C bonds, formed by the in-phase and out-of-phase d_σ orbitals of the $[Cp(CO)_2M]$ fragments interacting with the sp hybrid orbitals of the terminal carbon atoms. Together with $(x - 1)$ lower-lying orbitals describing the C–C σ bonds, not shown in the figures, they constitute the M–C_x–M σ skeleton. (ii) A group of closely spaced couples of levels originating from the interactions of the C_x p_π with the metal d_π orbitals. (iii) A few orbitals of δ symmetry built by the bonding and antibonding combinations of the d_{z^2} and d_{xz}, strongly mixed with ligand orbitals. These orbitals do not interact with any C_x p_π orbital and give no contribution to the bonding. (iv) A group of low-lying virtual orbitals which are essentially of d_δ–π*(CO) and d_δ–π*(Cp) character.

These results show that the calculated frontier orbitals of **9** and **10** correspond closely those of the proposed Hückel-like model (see above). In particular, the levels originating from the interactions of the C_x p_π with the metal d_π orbitals show the same nodal pattern and the same energy order expected on the basis of such a model, compare for instance Fig. 3 with the lower levels of Scheme 5. Moreover, a careful analysis of the composition of these π orbitals (see Tables 4 and 5) shows that the 1π orbitals have an almost pure $1\pi_u$ (C_4 or C_6) character and only the highest occupied π orbitals have a substantially mixed metal–carbon character. This justifies the assumption of the qualitative Hückel model, according to which the occupation of the highest molecular orbital of π character determines the valence description of the M–C and C–C bonds.

Table 3 Geometrical parameters, HOMO–LUMO gaps, Δ, HOMO energies, ε, and HOMO metal character, M (%), for $[\{Cp(CO)_2Fe\}_2(\mu\text{-}C_x)]$ and $(CH_3)_2(\mu\text{-}C_x)$ $x = 2$, 4, 6 or 8 compounds

Compound	Parameter	NLDA/Å	Δ/eV	ε/eV	M (%)
$[\{Cp(CO)_2Fe\}_2(\mu\text{-}C_2)]$	Fe–C (C_2)	1.924	1.80	−4.58	32
	C_α–C_β	1.231			
$[\{Cp(CO)_2Fe\}_2(\mu\text{-}C_4)]$	Fe–C (C_4)	1.900	1.59	−4.62	22
	C_α–C_β	1.230			
	C_β–C_γ	1.356			
$[\{Cp(CO)_2Fe\}_2(\mu\text{-}C_6)]$	Fe–C (C_6)	1.891	1.51	−4.76	17
	C_α–C_β	1.233			
	C_β–C_γ	1.342			
	C_γ–C_δ	1.232			
$[\{Cp(CO)_2Fe\}_2(\mu\text{-}C_8)]$	Fe–C (C_8)	1.887	1.50	−4.92	14
	C_α–C_β	1.235			
	C_β–C_γ	1.337			
	C_γ–C_δ	1.235			
	C_δ–C_ε	1.328			
$(CH_3)_2(\mu\text{-}C_2)$	C (Me)–C (C_α)	1.457	6.57	−6.39	
	C_α–C_β	1.211			
$(CH_3)_2(\mu\text{-}C_4)$	C (Me)–C (C_α)	1.445	4.56	−6.23	
	C_α–C_β	1.217			
	C_β–C_γ	1.355			
$(CH_3)_2(\mu\text{-}C_6)$	C (Me)–C (C_α)	1.441	3.50	−6.21	
	C_α–C_β	1.220			
	C_β–C_γ	1.343			
	C_γ–C_δ	1.228			
$(CH_3)_2(\mu\text{-}C_8)$	C (Me)–C (C_α)	1.440	2.85	−6.20	
	C_α–C_β	1.222			
	C_β–C_γ	1.339			
	C_γ–C_δ	1.232			
	C_δ–C_ε	1.330			

Geometries

The calculated C–C and M–C bond distances in the $[\{Cp(CO)_2M\}_2(\mu\text{-}C_x)]$ series ($x = 2$–8, M = Cr, Mn or Fe) including the dicationic iron species for $x = 4$ or 6 are reported in Tables 2 and 3. Note that all these geometrical parameters match very well with the model previously proposed, with the d^5, d^6 and d^7

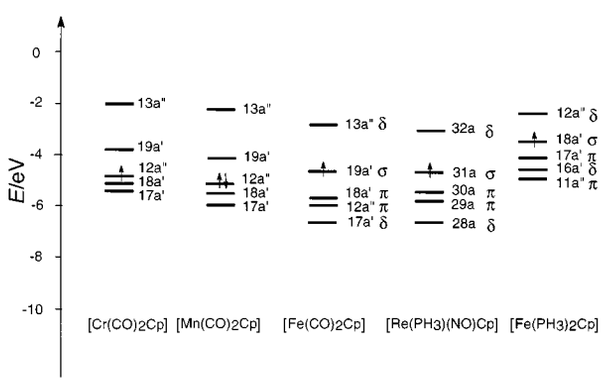

Fig. 2 Energies of the main frontier orbitals for the $[Cp(CO)_2M]$ metal fragments

Table 4 Energies and composition of the $[\{Cp(CO)_2Fe\}_2(\mu\text{-}C_4)]$ lowest unoccupied and highest occupied orbitals *

Orbital	ε/eV	Fe (%)	CO (%)	Cp (%)	C_4 (%)
$23a_g$	−2.77	31 ($3d_{x^2-y^2}$) + 11 ($3d_{xy}$)	13	17	
$22b_u$	−2.81	32 ($3d_{x^2-y^2}$) + 11 ($3d_{xy}$)		19	
$14b_g$	−2.97	44 ($3d_{xz}$)	13	20	
$14a_u$ LUMO	−3.03	43 ($3d_{xz}$)	15	28	
$13b_g$ HOMO (4π)	−4.62	22 ($3d_{yz}$)			69
$22a_g$ (4π)	−4.76	16 ($3d_{xy}$)			76
$13a_u$ (3π)	−6.23	56 ($3d_{yz}$)			22
$21b_u$ (3π)	−6.33	50 ($3d_{xy}$)		17	19
$21a_g$	−6.50	26 ($3d_{xy}$) + 25 ($3d_{z^2}$)	16		
$20b_u$	−6.85	39 ($3d_{z^2}$)	10		15
$12b_g$ (2π)	−6.95	51 ($3d_{yz}$)			20
$20a_g$ (2π)	−7.15	34 ($3d_{z^2}$) + 17 ($3d_{x^2-y^2}$) + 19 ($3d_{xy}$)			16
$19b_u$ (1π)	−7.53	11 ($3d_{z^2}$) + 12 ($3d_{x^2-y^2}$) + 2 ($3d_{xy}$)			74
$12a_u$ (1π)	−7.78	15 ($3d_{yz}$)			81
$11b_g$	−7.98	10 ($3d_{yz}$) + 11 ($3d_{xz}$)		60	
$11a_u$	−7.98	12 ($3d_{xz}$)		60	
$19a_g$	−8.16	17 ($3d_{xy}$)		42	
$18b_u$	−8.32	17 ($3d_{xy}$)		32	29
$18a_g$ (1σ)	−9.01	26 ($3d_{x^2-y^2}$)			38
$17b_u$ (1σ)	−9.24	24 ($3d_{x^2-y^2}$)			41

* Only the main contributions to each orbital have been given. The nature of metal contributions is mentioned in parentheses as well as the π nature of MOs.

Table 5 Energies and composition of the $[\{Cp(CO)_2Fe\}_2(\mu\text{-}C_6)]$ lowest unoccupied and highest occupied orbitals *

Orbital	ε/eV	Fe (%)	CO (%)	Cp (%)	C_6 (%)
$24a_g$	−3.01	32 ($3d_{x^2-y^2}$) + 11 ($3d_{xy}$)	18	10	
$24b_u$	−3.01	32 ($3d_{x^2-y^2}$) + 11 ($3d_{xy}$)	13	23	
$15a_u$	−3.19	44 ($3d_{xz}$)	17	25	
$14b_g$ LUMO	−3.24	43 ($3d_{xz}$)	15	15	
$14a_u$ HOMO (5π)	−4.75	17 ($3d_{yz}$)			75
$23b_u$ (5π)	−4.86	11 ($3d_{xy}$)			81
$13b_g$ (4π)	−6.17	42 ($3d_{yz}$)			39
$23a_g$ (4π)	−6.36	43 ($3d_{xy}$)			37
$22b_u$	−6.70	30 ($3d_{xy}$) + 24 ($3d_{z^2}$)	14	10	
$22a_g$	−6.87	37 ($3d_{z^2}$)			11
$13a_u$ (3π)	−6.97	51 ($3d_{yz}$)			24
$21b_u$ (3π)	−7.29	34 ($3d_{z^2}$) + 15 ($3d_{x^2-y^2}$) + 20 ($3d_{xy}$)	10		26
$21a_g$ (2π)	−7.53	21 ($3d_{z^2}$) + 16 ($3d_{x^2-y^2}$) + 12 ($3d_{xy}$)			27
$12b_g$ (2π)	−7.61	25 ($3d_{yz}$)			59
$20b_u$	−8.15	6 ($3d_{xy}$) + 8 ($3d_{x^2-y^2}$)		37	11
$12a_u$	−8.17	11 ($3d_{xz}$) + 11 ($3d_{yz}$)		59	
$11b_g$	−8.17	11 ($3d_{xz}$) + 10 ($3d_{yz}$)		60	
$20a_g$	−8.40	18 ($3d_{xy}$)		37	
$11a_u$ (1π)	−8.50	2 ($3d_{yz}$)			98
$19b_u$ (1π)	−8.65	10 ($3d_{xy}$)			70
$19a_g$ (1σ)	−9.42	24 ($3d_{x^2-y^2}$)			40
$18b_u$ (1σ)	−9.45	24 ($3d_{x^2-y^2}$)			40

* Only the main contributions to each orbital have been given. The nature of metal contributions is mentioned in parentheses as well as the π nature of MOs.

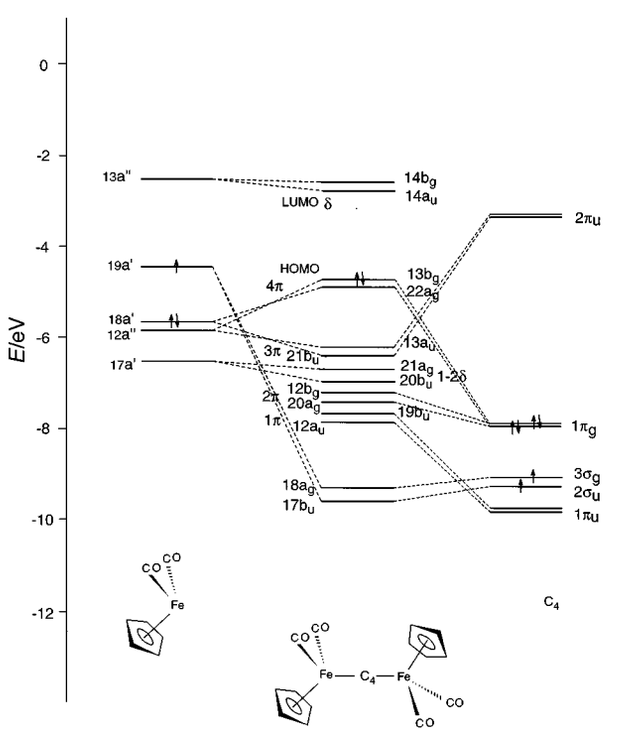

Fig. 3 Molecular orbital diagram for the $[\{Cp(CO)_2Fe\}_2(\mu\text{-}C_4)]$ complex depicting the interactions between the frontier orbitals of $[Cp(CO)_2Fe]$ and C_4

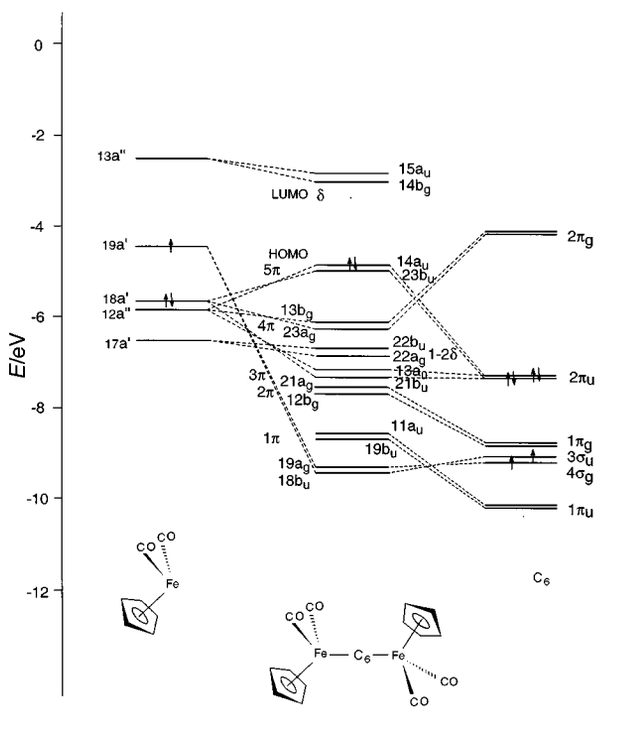

Fig. 4 Molecular orbital diagram for the $[\{Cp(CO)_2Fe\}_2(\mu\text{-}C_6)]$ complex depicting the interactions between the frontier orbitals of $[Cp(CO)_2Fe]$ and C_6

configurations of the $[Cp(CO)_2M]$ metal fragments leading, respectively, to polyynic **A**, cumulenic **B** and polyynic **C**, valence descriptions (see Scheme 3). The iron C_x bridged (x = 2–8) complexes show polyynic structures **A**, with alternating single and triple bonds, starting with a Fe–C single bond. Cumulenic structures **B** have been obtained for the C_x bridged complexes of manganese and for the dicationic iron complexes with a slightly alternating short/long pattern which reproduces that observed for $[\{Cp^*Re(NO)(PPh_3)\}_2(\mu\text{-}C_4)]^{2+}$.[29] Polyynic structures **C** have been calculated for four or six carbon-bridged complexes of chromium, with alternating single and triple bonds, starting with Cr–C triple bonds. Table 2 clearly illustrates that going from Cr to Fe in the $[\{Cp(CO)_2M\}_2(\mu\text{-}C_4)]$ series {*i.e.* going from a d^5 to a d^7 configuration of the $[Cp(CO)_2M]$ fragment} there is a lengthening of the $M\text{–}C_\alpha$ bond and simultaneous shortening and lengthening of the $C_\alpha\text{–}C_\beta$ and $C_\beta\text{–}C_\gamma$ bonds, respectively. An analogous trend is observed for the $[\{Cp(CO)_2M\}_2(\mu\text{-}C_6)]$ series. We must take into account that to assign the calculated C–C bond lengths to single, double or triple C–C bonds the right comparison should be made with single, double, and triple bonds between sp

hybridized carbons. So, for a (MC). . .–C≡C–. . .(CM) triple bond the most pertinent comparison can be made with ethyne (1.212 Å), for a (MC). . .=C=C=. . .(CM) double bond such a comparison is provided by the central C–C distance in buta-1,2,3-triene (1.284 Å) and for a (MC). . .≡C–C≡. . .(CM) single bond by the central C–C distance in buta-1,3-diyne (1.384 Å). Therefore, we assigned carbon–carbon single, double and triple bonds to C–C distances in the range 1.32–1.34, 1.27–1.30 and 1.23–1.26 Å, respectively. More difficult is the assignment of the M–C bond orders on the basis of the optimized M–C bond lengths because of the limited available experimental data. However, we can say that the Cr–C bond distance of 1.746 Å is in the range of distances expected for the Cr–C triple bonds, 1.65–1.79 Å, while the Fe–C distance of 1.90 Å is in the range of single Fe–C bonds, with a sp hybridized carbon (1.90 Å).[60] The Mn–C bond distance of 1.80 Å has a value which can be reasonably assigned to a double bond. The Fe–C bond distance in the dicationic complexes of 1.79 Å has a value close to experimentally observed double Fe^{+}–C bonds {*e.g.* 1.81 Å in $[(CO)_2CpFe{=}CCl_2]^{+}$[61]}. Finally, in Table 3 we compare the optimized geometrical parameters of the $[\{Cp(CO)_2Fe\}_2(\mu\text{-}C_x)]$ and $(CH_3)_2(\mu\text{-}C_x)$ species ($x = 2$, 4, 6 or 8). We notice that on lengthening the C_x chain from $x = 2$ to $x = 8$ the agreement between the C–C bond distances in the two series improves, as expected because of the diminished effect of the terminal metal fragments.

Metal-chain interactions and bridge length

The orbital interaction diagrams of **9** and **10** in Figs. 3 and 4 illustrate the most relevant interactions between the metal fragment d_π orbitals and the π system of the C_4 and C_6 bridging units. We can distinguish two main interactions: (i) a filled–filled interaction between the d_π orbitals 18a′ 12a″ and the $1\pi_g$ (C_4) or $2\pi_u$ (C_6) bridge orbitals; and (ii) a filled–empty interaction between the same d_π orbitals 18a′ 12a″ and the $2\pi_u$ (C_4) or $2\pi_g$ (C_6) orbitals. The HOMO orbital is composed mainly of the highest occupied bridge orbitals, $1\pi_g$ (C_4) or $2\pi_u$ (C_6), strongly mixed (in an antibonding fashion) with the metal d_π orbitals. The LUMO is composed primarly of the metal d_δ orbital, 13a″(d_{xz}).

Due to the filled–filled interaction, the HOMO in the considered dinuclear complexes is significantly higher in energy than the HOMO of the polyyne bridge (see Figs. 3 and 4), this explains the red shift of the UV maxima in these complexes from those of the analogous methylated polyynes. An analogous effect has been established by photoelectron spectroscopy for many alkynyl complexes.[62] Moreover, the nature of HOMO and LUMO suggests for these UV transitions a bridge to metal charge-transfer character, in agreement with their higher intensities than in the analogous methylated polyynes.

On lengthening the bridging chain from C_4 to C_8, several effects are observed as shown in Table 3: (i) the HOMO–LUMO gap decreases, in agreement with the experimental UV/VIS spectra for the $[\{Cp^*Re(PPh_3)(NO)\}_2(\mu\text{-}C_x)]$ compounds which exhibit progressively red-shifted bands.[31] The decrease is less pronounced than for the analogous methylated polyynes due to the high metal character of the LUMO and, to a lesser extent, of the HOMO orbitals. (ii) The metal character of the HOMO orbital decreases thus leading to a more marked bridge to metal character of the lowest electronic transition, in agreement with the increasing intensities of the UV/VIS bands of the $[\{Cp^*Re(PPh_3)(NO)\}_2(\mu\text{-}C_x)]$ compounds.[31] (iii) The HOMO energies of the considered dinuclear complexes decrease (see Table 3) in agreement with the experimental evidence that oxidations become thermodynamically less favourable in the $[\{Cp^*Re(PPh_3)(NO)\}_2(\mu\text{-}C_x)]$ series as the carbon chain increases from C_4 to C_{20}.[30] Although this trend seems at first counter intuitive (since the HOMO energies of the organic polyynes increase as conjugation is extended), it can be rationalized on the basis of the nature of the HOMO in these dinuclear complexes. As discussed above, these HOMOs originate from the filled–filled interaction between the fragment d_π orbitals and the polyyne HOMOs and are therefore significantly higher than the latter bridge orbitals. As the polyyne HOMO energies increase with the chain length, their filled–filled interaction with the d_π orbitals diminishes so that the HOMO energies of the dinuclear complexes (which are the antibonding component of such an interaction) decrease. This view is supported by the decrease of the metal character of the HOMOs on lengthening the bridging chain.

Table 6 Comparison between the optimized geometrical parameters of the $[\{Cp(CO)_2Fe\}_2(\mu\text{-}C_4)]$ and (*SS*,*RR*)-$[\{Cp(NO)(PH_3)Re\}_2(\mu\text{-}C_4)]$ model complexes with the crystallographic data for (*SS*,*RR*)-$[\{Cp^*(NO)(PPh_3)Re\}_2(\mu\text{-}C_4)]$

Complex	M–C_α/Å	C_α–C_β/Å	C_β–C_γ/Å
$[\{Cp(CO)_2Fe\}_2(\mu\text{-}C_4)]$	1.900	1.230	1.356
(*SS*,*RR*)-$[\{Cp(NO)(PH_3)Re\}_2(\mu\text{-}C_4)]$	2.033	1.234	1.350
(*SS*,*RR*)-$[\{Cp^*(NO)(PPh_3)Re\}_2(\mu\text{-}C_4)]$	2.037	1.202	1.389

Comparison with the experimentally synthesized compounds

The above formal structures, forecast by the proposed Hückel-like model and obtained by our accurate DFT calculations, coincide with those which appear in the diagram of representative redox states (Scheme 3).[29] These structures agree with all the geometries experimentally observed for the several complexes of the $[\{Cp^*Re(PPh_3)(NO)\}_2(\mu\text{-}C_x)]^{z+}$ series,[19,20,27–30] although no oxidized form with the **C** structure, M(–C≡C–)$_{x/2}$-M, has been isolated yet. Also the dependence of the HOMO–LUMO gap and HOMO and LUMO nature and energies on chain length, calculated for the $[\{CpFe(CO)_2\}_2(\mu\text{-}C_x)]$ complexes, is in agreement with the experimental behaviour observed for the Gladysz series, as discussed above. This stems from the similar orbital energies of the isoelectronic $[Cp(CO)_2Fe]$ and $[Cp^*Re(PPh_3)(NO)]$ (d^7) endgroups, see Fig. 2. Moreover, an explicit DFT calculation has been carried out on the $[\{CpRe(NO)(PH_3)_2\}_2(\mu\text{-}C_4)]$ model complex **11** in which the Cp* and PPh_3 ligands of the real complex have been replaced by a Cp and a PH_3 molecule, respectively. A geometry optimization of this molecule led to a polyynic structure very close to that obtained for the bimetallic complex **9** with $[CpFe(CO)_2]$ endgroups and in fairly good agreement with the experimentally determined crystal structure, see Table 6. The computed valence energy levels of **11** are also analogous to those of **9** with a HOMO of $1\pi_g$ (C_4) character significantly mixed in an antibonding fashion with the metal d_π orbitals (*i.e.* a 4π in the Hückel-like model).

A different behaviour is found for the $[\{Cp^*Fe(dppe)\}_2(\mu\text{-}C_x)]^{z+}$ series.[32–34] Indeed, although the neutral complexes of this series show a polyyne-like structure, as expected for a d^7 ending group, IR data suggest that the doubly ionized species still have a polyyne-like structure rather than the expected cumulene-like one. This anomaly can be rationalized by a slight generalization of the above electron count scheme which takes into account the different nature of the metal fragment. Indeed, while in the $[\{CpFe(CO)_2\}_2(\mu\text{-}C_x)]$ complexes, and presumably also in the similar $[\{Cp^*Re(PPh_3)(NO)\}_2(\mu\text{-}C_x)]^{z+}$ species, the HOMO is a $(\frac{x}{2} + 2)\pi$ orbital (*i.e.* 4π for C_4, 5π for C_6, *etc.*, see Tables 4 and 5) with the δ orbitals slightly lower, in the $[\{Cp^*Fe(dppe)\}_2(\mu\text{-}C_x)]$ complexes, where the iron fragment is co-ordinated by stronger σ-donor phosphine ligands, the δ orbitals are destabilized and expected to be the HOMO. Therefore, double ionization of the latter complex leads to a depopulation of the δ orbital and does not change the polyynic structure. This is confirmed by a DFT calculation performed on the $[CpFe(PH_3)_2]$ fragment which shows a significant destabilization of the d_δ orbitals, see Fig. 2.

Table 7 Contributions to the total bonding energy (eV) from different symmetries for the decomposition of iron complexes (C_{2h} symmetry) into C_2, C_4, C_6 and C_8 and the corresponding metal fragments

	[{Cp(CO)$_2$Fe}$_2$(μ-C$_x$)]			
	$x = 2$	$x = 4$	$x = 6$	$x = 8$
ΔE_{Ag}	−10.3	−8.7	−10.9	−8.2
ΔE_{Bg}	−0.4	−0.2	−0.6	−0.3
ΔE_{Au}	−0.1	−0.5	−0.3	−0.6
ΔE_{Bu}	−8.5	−10.8	−8.3	−10.9
$\Delta E^o + \Delta E_{oi}$	−9.1	−9.7	−9.5	−9.4

Such a result supports the diradical $^{+\bullet}$Fe–C≡C–C≡C–Fe$^{\bullet+}$ valence structure suggested for the $[\{CpFe(PH_3)_2\}_2(\mu\text{-}C_4)]^{2+}$ species.[29]

Energy decomposition and bond analysis

In the discussion of the bonding in these complexes, it is useful to point out the relative magnitudes of the main interactions and the strengths of the bond between the two metal fragments and the central C_x unit.

A better insight into the electronic factors governing the relative stability of the [{Cp(CO)$_2$M}$_2$(μ-C$_x$)] complexes is provided by the analysis of the orbital interaction energy in terms of the different symmetries [equation (1)]. An analysis of the

$$\Delta E_{oi} = \sum_{\Gamma} \Delta E_{\Gamma} \qquad (1)$$

interaction energies in terms of σ and π contributions is not straightforward as, in the C_{2h} symmetry group, σ and π components mix in the A_g and B_u symmetries. Such an analysis is however quite simple for the series of iron complexes ($x = 2$, 4, 6 or 8), shown in Table 7, for which no π contribution is expected and ΔE_{Ag} and ΔE_{Bu} represent the contributions to ΔE_{oi} due to the pure metal–carbon σ interactions. We see that the metal–carbon interaction energy remains essentially constant on increasing the chain length. This supports the expectation that there may be no practical upper limit on chain length[29] based on the analogy with the recent data for sp carbon chains with organic endgroups.[63]

For the chromium and manganese complexes, in addition, there are substantial contributions due to the back donation from the metal to the antibonding π* orbitals of C_x and contributions due to the donation from the C_x highest occupied π orbitals to the empty metal orbitals. However, these effects contribute simultaneously to all four different symmetries of the C_{2h} group and give therefore less direct information. The results of this analysis for the [{Cp(CO)$_2$M}$_2$(μ-C$_x$)] (M = Cr, Mn or Fe) series of complexes with $x = 4$ and 6 are reported in Table 8. We see that for all the complexes a substantial contribution to thermodynamic stability comes from the π bonding which varies considerably shifting from Fe to Cr in agreement with the change of the valence structures from **A** to **C**. In particular, the overall bonding energy increases on going from Fe to Cr in agreement with the increase of the formal metal–carbon bond order, but does not change on increasing the chain length from C_4 to C_6.

Metal–metal communication

An estimate of the extent of metal–metal interaction through the carbon bridge can be obtained by electrochemistry.[64] Indeed, such $L_mMC_xML_m$ dinuclear complexes undergo two separate reversible oxidations, corresponding to two one-electron processes shown in equation (2) leading to two oxid-

$$[L_mMC_xML_m] \xrightarrow{-e} [L_mMC_xML_m]^+ \xrightarrow{-e} [L_mMC_xML_m]^{2+} \qquad (2)$$

Table 8 Contributions to the total bonding energy (eV) from different symmetries for the decomposition of chromium, manganese and iron complexes (C_{2h} symmetry) into C_4 and C_6 and the corresponding metal fragments

	[{Cp(CO)$_2$M}$_2$(μ-C$_4$)]			[{Cp(CO)$_2$M}$_2$(μ-C$_6$)]		
	Cr	Mn	Fe	Cr	Mn	Fe
ΔE_{Ag}	−0.5	−4.7	−8.7	−16.3	−14.9	−10.9
ΔE_{Bg}	3.3	4.5	−0.2	−8.0	−1.3	−0.6
ΔE_{Au}	−7.7	−1.2	−0.5	3.4	4.5	−0.3
ΔE_{Bu}	−16.1	−14.6	−10.8	0.1	−4.3	−8.3
$\Delta E^o + \Delta E_{oi}$	−12.2	−10.3	−9.7	−12.0	−10.0	−9.5

Table 9 Experimental differences between the first (E_1^o) and second (E_2^o) oxidation potentials, ΔE^o and available effective coupling parameters, V_{ab}, measured for the synthesized rhenium and iron complexes

	ΔE^o/V	V_{ab}/eV
[{Cp*Re(NO)(PPh$_3$)}$_2$(μ-C$_4$)]	0.53	0.70
[{Cp*Re(NO)(PPh$_3$)}$_2$(μ-C$_6$)]	0.38	
[{Cp*Re(NO)(PPh$_3$)}$_2$(μ-C$_8$)]	0.29	
[{Cp*Re(NO)(PPh$_3$)}$_2$(μ-C$_{12}$)]	0.19	
[{Cp*Re(NO)(PPh$_3$)}$_2$(μ-C$_{16}$)]	0.09	
[{Cp*Re(NO)(PPh$_3$)}$_2$(μ-C$_{20}$)]	0.00	
[{Cp*Fe(dppe)}$_2$(μ-C$_4$)]	0.72	0.47
[{Cp*Fe(dppe)}$_2$(μ-C$_8$)]	0.43	0.32

ation peaks in the cyclic voltammograms.[30,33] In the absence of any electron coupling, the two identical metal centers are expected to undergo oxidation at the same oxidation potential. Any communication across the bridge moves the second metal ion to perceive the additional positive charge and leads to a difference ($\Delta E^o = E_2^o - E_1^o$) between the two oxidation potentials. Such a difference stabilizes the mixed valence, partially oxidized species which comproportionates in solution according to the following equilibrium (3) whose comproportionation constant

$$[L_mMC_xML_m] + [L_mMC_xML_m]^{2+} \rightleftharpoons 2[L_mMC_xML_m]^+ \qquad (3)$$

is an alternative estimate of the metal–metal interaction.[64]

Cyclic voltammograms of [{Cp*Re(NO)(PPh$_3$)}$_2$(μ-C$_x$)] complexes (x = 4–20) show two chemical reversible one-electron oxidations for $x \leqslant 16$, and for $x = 20$ only a single two-electron oxidation is observed.[30] The values of the oxidation potential differences for this series of complexes are reported in Table 9 and show a decrease from 0.53 V for $x = 4$ to 0.09 V for $x = 16$. An analogous behaviour is observed in the [{Cp*Fe(dppe)}$_2$(μ-C$_x$)] complexes (x = 4–8) for which slightly higher potential differences are observed, and a remarkably high value is still observed for the largest synthesized C_8 chain (ΔE^o = 0.43 V).[34]

A study of the $[\{CpFe(CO)_2\}_2(\mu\text{-}C_x)]^+$ species can elucidate the extent of the metal–metal interaction. According to the electron count assumed in this work, these species have been considered as constituted by d^7 and d^6 metal fragments. However, according to the usual oxidation state formalism, these molecules are generally considered as Fe^{II}–Fe^{III}, d^6–d^5, mixed-valence species. Many d^6–d^5 mixed-valence systems are known,[65,66] specially for ruthenium, and can exhibit localized, partially delocalized or fully delocalized electronic structures (class I, II and III according to Robin and Day[67]). If the metal–metal interaction is very strong, the odd electron of the mixed valence state occupies a molecular orbital completely delocalized over the metal–bridge–metal system and is evenly distributed between the two metals (class III). If the metal–metal interaction is weaker, the odd electron is localized on one of the metals and an energy barrier is needed for transferring the electron from the metal in the lower oxidation state to the other metal (class II).[65–68] As an odd electron can be studied

by magnetic and spectroscopic investigations and its valence trapping can easily be determined by several spectroscopic techniques, the study of the mixed valence species is the best way to determine the efficiency of the bridging ligand in promoting metal–metal interactions. In all cases where a monocationic C_x bridged dinuclear species has been isolated[33,35] (rhenium and iron series), IR, ESR and, for the iron complexes, Mössbauer spectra showed that the odd electron is fully delocalized between the two metals (class III).

Our calculations on the $[\{Cp(CO)_2Fe\}_2(\mu\text{-}C_x)]^+$ ($x = 4$–8) series of complexes (see Table 1) are in agreement with these findings as the singly occupied MO is fully delocalized over the metals and all the carbon atoms of the bridge. That these ions can be considered as class III mixed-valence species has been confirmed by broken-symmetry calculations. Geometry optimizations were performed on the $[\{Cp(CO)_2Fe\}_2(\mu\text{-}C_x)]^+$ ($x = 4$–8) complexes with a broken symmetry approach, *i.e.* removing the inversion center between the two metal fragments and lowering the symmetry from the C_{2h} molecular symmetry to C_s (see Computational and Methodological Details section). These optimizations were started from an asymmetric initial geometry where the co-ordination sphere on the left metal was taken from the optimized geometry for neutral $[\{Cp(CO)_2Fe\}_2(\mu\text{-}C_x)]$ and that on the right metal was taken from the optimized geometry for the corresponding dicationic species. This initial geometry would simulate the localization of the positive charge, and correspond to a localized Fe^{II}–Fe^{III} valence structure. For a localized (class I or class II) mixed-valence compound an asymmetric optimized geometry close to the above initial geometry would be expected. An essentially symmetric optimized geometry is instead obtained for all these monocationic species, with M–C and C–C bond lengths intermediate between those of the neutral and dicationic species; Table 10 illustrates the results for the longest considered chain with $x = 8$. This result indicates that the potential energy curve as a function of the vibrational coordinate Q (representing the antisymmetric breathing of the co-ordination spheres), conventionally used to describe mixed-valence systems, presents a minimum in $Q = 0$ which is the formal condition for class III compounds.

In order to give a theoretical quantitative estimate of the metal–metal interaction in the $[\{Cp(CO)_2Fe\}_2(\mu\text{-}C_x)]$ complexes and its dependence on the chain length, we calculated the difference between the first and second gas-phase ionization potentials, $\Delta IP = IP([L_mMC_xML_m]^+) - IP([L_mMC_xML_m])$. This quantity is strictly related to the experimental parameter usually considered to estimate the extent of metal–metal interaction in dinuclear bridged complexes, the difference between the first and second oxidation potentials ΔE^o, and offers the advantage of being independent from the complex–solvent interactions which operate in solution. Indeed, the standard redox potentials for each of the two successive one-electron reductions, E_1^o or E_2^o, can be, in principle, evaluated by adding to the gas phase ionization potential for the reduced species the solvation energy differences for the oxidized minus the reduced state. A known constant potential has to be added to reference the obtained potential to the considered standard electrode. The final expressions are given in equations (4) and (5) so that we can write equation (6).

$$E_1^o = IP([L_mMC_xML_m]) + E_{solv}([L_mMC_xML_m]) - E_{solv}([L_mMC_xML_m]^+) + \text{const} \quad (4)$$

$$E_2^o = IP([L_mMC_xML_m]^+) + E_{solv}([L_mMC_xML_m]^{2+}) - E_{solv}([L_mMC_xML_m]^+) + \text{const} \quad (5)$$

$$\Delta E^o = \Delta IP + E_{solv}([L_mMC_xML_m]^{2+}) - E_{solv}([L_mMC_xML_m]) \quad (6)$$

Table 10 Optimized geometrical parameters for the $[\{Cp(CO)_2Fe\}_2(\mu\text{-}C_8)]^{z+}$ neutral, monocationic and dicationic species

Complex	M–C_α/Å	C_α–C_β/Å	C_β–C_γ/Å	C_γ–C_δ/Å	C_δ–C_ε/Å
$[\{Cp(CO)_2Fe\}_2(\mu\text{-}C_8)]$	1.887	1.235	1.337	1.235	1.328
$[\{Cp(CO)_2Fe\}_2(\mu\text{-}C_8)]^+$	1.837	1.249	1.314	1.249	1.305
$[\{Cp(CO)_2Fe\}_2(\mu\text{-}C_8)]^{2+}$	1.794	1.266	1.295	1.263	1.288

Table 11 Differences between the first (IP_1) and second (IP_2) ionization energies and effective coupling parameters (V_{ab}) calculated for the considered iron complexes

	$\Delta E = IP_2 - IP_1$/eV	V_{ab}/eV
$[\{Cp(CO)_2Fe\}_2(\mu\text{-}C_2)]$	4.44	0.85
$[\{Cp(CO)_2Fe\}_2(\mu\text{-}C_4)]$	4.12	0.79
$[\{Cp(CO)_2Fe\}_2(\mu\text{-}C_6)]$	3.82	0.73
$[\{Cp(CO)_2Fe\}_2(\mu\text{-}C_8)]$	3.54	0.64

The ionization potentials have been obtained *via* a Δ_{DFT} calculation as the difference in total energy between the reduced species in the unionized initial state and in the ionized final state and the results are reported in Table 11. To check the reliability of these values, we evaluated approximately ΔE^o in dichloromethane using a rough estimate of the solvation energies *via* the simple electrostatic Born model[69] [equation (7)] where Q is the

$$E_{solv} = -\frac{Q}{2R_{eff}}\left(1 - \frac{1}{\varepsilon}\right) \quad (7)$$

total molecular charge, ε is the solvent relative permittivity and R_{eff} is the effective molecular radius of the molecule. The term R_{eff} can be approximated to the radius of the spherical cavity encompassing the van der Waals envelope around the atoms. For the C_4 complexes (whose electrostatic potential is expected to be better approximated by a spherical model) we calculate a solvation energy contribution of *ca.* −3.4 eV ($R_{eff} = 11.4$ Å, $\varepsilon = 9.1$) which would lead to a ΔE^o of 0.7 V, a value remarkably close to the experimental values of 0.53 V for $[\{Cp^*Re(NO)(PPh_3)\}_2(\mu\text{-}C_4)]$[19] and 0.72 V for $[\{Cp^*Fe(dppe)\}_2(\mu\text{-}C_4)]$.[33]

For all the considered systems, the calculated gas phase values of ΔIP have high positive values while large negative solvation energy differences are instead expected (compare −3.4 eV approximately calculated for the C_4 complex) due to the much stronger solvation of the more positively charged species, leading to the small oxidation potentials observed in solution. Note that the relative decrease of ΔIP on lengthening the carbon chain is less pronounced than the decrease of the experimental ΔE^o (see Table 9 and 11) and that the value calculated for the C_8 species is still quite high (3.54 eV) suggesting that a high metal–metal interaction still operates through the C_8 bridge.

The high electronic communication between metal endgroups in this C_8-bridged dinuclear complex is consistent with the broken symmetry calculations performed on the monocationic $[\{Cp(CO)_2Fe\}_2(\mu\text{-}C_8)]^+$ species which proves the fully delocalized nature of this mixed-valence compound (see above).

The extent of the metal–metal interaction in a mixed valence dinuclear complex is often expressed in terms of the effective coupling parameter V_{ab}. Such a quantity corresponds to the perturbation Hamiltonian which couples the states related by electron transfer between the two metals and can be obtained from the experimental data through the Hush formula.[70] For a strongly delocalized mixed-valence compound (class III), it can be obtained as half the transition energy of the intervalence charge transfer (IVCT) band. According to the 'dimer splitting' method of ref. 71, we evaluated V_{ab} as half of the energy difference between the two MOs which correspond to the in-phase and out-of-phase combinations of the d_π orbitals separated due

to the interaction with the bridge π system. For our polyyne-bridged complexes, we have two couples of such split MOs corresponding to the metal–metal interaction through the π_x and π_y delocalized systems of the bridge, *e.g.* $13a_u$–$13b_g$ and $21b_u$–$22a_g$ for the C_4 complex. Due to the low C_{2h} symmetry, two slightly different energy separations are obtained of which we took the average value. The results for the C_4, C_6 and C_8 complexes are reported in Table 11 which shows high V_{ab} values, greater than 0.5 eV, corresponding to a strong coupling between the two metals even for the longest considered C_8 chain. These values therefore indicate strongly delocalized mixed-valence behaviour for the monocationic species and are of the same order of magnitude of the experimental values for some of the synthesized compounds, *e.g.* 0.70 eV for $[\{Cp^*Re(PPh_3)(NO)\}_2(\mu\text{-}C_4)]$,[29] 0.47 eV for $[\{Cp^*Fe(dppe)\}_2(\mu\text{-}C_4)]$[33] and 0.32 eV for $[\{Cp^*Fe(dppe)\}_2(\mu\text{-}C_8)]$,[34] see Table 9.

These results show a high metal–metal electronic communication for the considered C_4–C_8 species suggesting that even longer C_x chains can act as a molecular wire connecting the two metal centers.

Conclusion

In the present investigation we have studied the electronic and geometrical structures of C_x bridged dinuclear complexes. Compounds with an even C_x bridge are much more common and three valence formulations are possible, *i.e.* polyyne-like $M(-C\equiv C-)_{x/2}M$, cumulene-like $M(=C=C=)_{x/2}M$, and polyyne-like $M(\equiv C-C\equiv)_{x/2}M$.

Density functional calculations have been performed on a $[\{Cp(CO)_2Fe\}_2(\mu\text{-}C_x)]$ (M = Cr, Mn or Fe; $x = 4$–8) series of even C_x bridged dinuclear complexes close to several experimental compounds. These calculations showed that the geometrical structure is essentially determined by the nodal pattern of the highest molecular orbitals of d_π–p_π (C_x) character. On the basis of such results we have developed a simple molecular orbital model which allows the prediction of the valence formulation in these dinuclear complexes.

As long as d_δ orbitals are not too high in energy, the following order can be used to forecast the valence formulations on the basis of the d^n configurations of the endgroups: d^5 $M(\equiv C\text{–}C\equiv)_{x/2}M$, d^6 $M(=C=C=)_{x/2}M$, d^7 $M(-C\equiv C-)_{x/2}M$, and these structures are formally related by two-electron oxidations. When, due to strong σ donating ligands, the d_δ orbitals lie much higher in energy than the d_π orbitals only the following polyyne-like structures have been calculated: d^5 $M(-C\equiv C-)_{x/2}M$, d^6 $^\bullet M(-C\equiv C-)_{x/2}M^\bullet$, d^7 $M(-C\equiv C-)_{x/2}M$.

We propose to use the difference between the first and second gas-phase ionization potentials, $\Delta IP = IP([L_mMC_xML_m]^+) - IP([L_mMC_xML_m])$, as a parameter to estimate the metal–metal interaction in these dinuclear complexes. This quantity is strictly related to the experimental parameter usually considered in estimating the extent of metal–metal interactions in dinuclear bridged complexes, the difference between the first and second oxidation potentials ΔE^o, and has the advantage of being independent from the strong complex–solvent interactions which operate in solution. The calculated gas phase values of ΔIP have high positive values for all the considered complexes up to C_8. Although a significant decrease of ΔIP on lengthening is calculated, the value obtained for the C_8 species is still quite high (3.54 eV) suggesting that a significant metal–metal interaction could operate even for very long bridging chains.

Acknowledgements

The present work has been carried out within the COST (European Program for Scientific Research) D3 Action. One of us (N. R.) thanks the Fundation Herbette, University of Lausanne (Switzerland), for providing a grant. Support by the Fonds National Suisse de la Recherche Scientifique (Bern, Switzerland, Grant no. 20-46590.96) and the Consiglio Nazionale della Ricerche (Rome, Italy) is gratefully acknowledged. Thanks are due to the Centro di Colcolo Interuniversitario dell'Italia Nord-Orientale (Bologna, Italy) for a computational grant.

References

1 F. Diederich and Y. Rubin, *Angew. Chem.*, *Int. Ed. Engl.*, 1992, **31**, 1101.
2 H. Lang, *Angew. Chem.*, *Int. Ed. Engl.*, 1994, **34**, 547.
3 W. Beck, B. Niemer and M. Wieser, *Angew. Chem.*, *Int. Ed. Engl.*, 1993, **32**, 923 and refs. therein.
4 M. Akita and Y. Moro-oka, *Bull. Chem. Soc. Jpn.*, 1995, **68**, 420.
5 U. Bunz, *Angew. Chem.*, *Int. Ed. Engl.*, 1996, **35**, 969.
6 D. R. Neithamer, R. E. LaPointe, R. A. Wheeler, D. S. Richeson, G. D. Van Duyne and P. T. Wolczanski, *J. Am. Chem. Soc.*, 1989, **111**, 9056.
7 K. G. Caulton, R. H. Cayton, R. H. Chisholm, J. C. Huffman, E. B. Lobkovsky and Z. Xue, *Organometallics*, 1992, **11**, 321.
8 S. De Angelis, E. Solari, C. Floriani, A. Chiesi-Villa and R. Rizzoli, *Angew. Chem.*, *Int. Ed. Engl.*, 1995, **34**, 1092.
9 P. Binger, P. Müller, P. Philipps, B. Gabor, R. Mynott, A. T. Herrmann, F. Langhauser and C. Krüger, *Chem. Ber.*, 1992, **125**, 2209.
10 J. Heidrich, M. Stelman, M. Appel, W. Beck, J. R. Phillips and W. C. Trogler, *Organometallics*, 1990, **9**, 1296.
11 J. A. Davies, M. El-Ghanam, A. A. Pinkerton and D. A. Smith, *J. Organomet. Chem.*, 1991, **409**, 367.
12 G. A. Koutsantonis and J. P. Selegue, *J. Am. Chem. Soc.*, 1991, **113**, 2316.
13 F. R. Lemke, D. J. Szalda and R. M. Bullock, *J. Am. Chem. Soc.*, 1991, **113**, 8466.
14 M. C. Chen, Y. J. Tsai, C. T. Chen, Y. C. Lin, T. W. Tseng, G. H. Lee and Y. Wang, *Organometallics*, 1991, **10**, 378.
15 N. A. Ustynyuk, U. N. Vinogradova and D. N. Kravtsov, *Organomet. Chem. USSR*, 1988, **1**, 45.
16 H. Ogawa, K. Onitsuka, T. Joh, S. Takahashi, Y. Yamamoto and H. Yamazaki, *Organometallics*, 1988, **7**, 2257.
17 R. J. Cross and M. F. Davidson, *J. Chem. Soc.*, *Dalton Trans.*, 1986, 411.
18 M. Akita, M. Terada, S. Oyama, S. Sugimoto and Y. Moro-oka, *Organometallics*, 1991, **10**, 1561.
19 Y. Zhou, J. W. Seyler, W. Weng, A. M. Arif and J. A. Gladysz, *J. Am. Chem. Soc.*, 1993, **115**, 8509.
20 J. W. Seyler, W. Weng, Y. Zhou and J. A. Gladysz, *Organometallics*, 1993, **12**, 3802.
21 R. Crescenzi and C. Lo Sterzo, *Organometallics*, 1992, **11**, 2301.
22 T. Rappert, O. Nürnberg and H. Werner, *Organometallics*, 1993, **12**, 1359.
23 M. I. Bruce, P. Hinterding, E. R. T. Tieking, B. W. Skelton and A. H. White, *J. Organomet. Chem.*, 1993, **450**, 209.
24 V. W. W. Yam, C. Y. Lau and K. K. Cheung, *Organometallics*, 1996, **15**, 1740.
25 O. Gevert, J. Wolf and H. Werner, *Organometallics*, 1996, **15**, 2806.
26 E. Viola, C. Lo Sterzo and F. Trezzi, *Organometallics*, 1996, **15**, 4352.
27 W. Weng, T. Bartik, M. Brady, B. Bartik, J. A. Ramsden, A. M. Arif and J. A. Gladysz, *J. Am. Chem. Soc.*, 1995, **117**, 11 922.
28 M. Brady, W. Weng and J. A. Gladysz, *J. Chem. Soc.*, *Chem. Commun.*, 1994, 2655.
29 M. Brady, W. Weng, Y. Zhou, J. W. Seyler, A. J. Amoroso, A. M. Arif, M. Böeme, G. Frenking and J. A. Gladysz, *J. Am. Chem. Soc.*, 1997, **119**, 775.
30 T. Bartik, B. Bartik, M. Brady, R. Dembinski and J. A. Gladysz, *Angew. Chem.*, *Int. Ed. Engl.*, 1996, **35**, 414.
31 B. Bartik, R. Dembinski, T. Bartik, A. M. Arif and J. A. Gladysz, *New J. Chem.*, 1997, **21**, 739.
32 N. Le Narvor and C. Lapinte, *J. Chem. Soc.*, *Chem. Commun.*, 1993, 357.
33 N. Le Narvor, L. Toupet and C. Lapinte, *J. Am. Chem. Soc.*, 1995, **117**, 7129.
34 F. Coat and C. Lapinte, *Organometallics*, 1996, **15**, 477.
35 W. Weng, A. M. Arif and J. A. Gladysz, *Angew. Chem.*, *Int. Ed. Engl.*, 1993, **32**, 891.
36 C. Hartbaum, G. Roth and H. Fischer, *Chem. Ber./Recl.*, 1997, **130**, 479.
37 W. Weng, J. A. Ramsden, A. M. Arif and J. A. Gladysz, *J. Am. Chem. Soc.*, 1993, **115**, 3824.

38 W. Weng, T. Bartik and J. A. Gladysz, *Angew. Chem.*, *Int. Ed. Engl.*, 1994, **33**, 2199.
39 B. E. Woodworth and J. L. Templeton, *J. Am. Chem. Soc.*, 1996, **118**, 7418.
40 J. R. Heath, Q. Zhang, S. C. O'Brien, R. F. Curl, N. W. Kroto and R. E. Smalley, *J. Am. Chem. Soc.*, 1987, **109**, 359.
41 Q. Fan and G. V. Pfeiffer, *Chem. Phys. Lett.*, 1989, **162**, 472.
42 P. Belanzoni, N. Re, M. Rosi, A. Sgamellotti and C. Floriani, *Organometallics*, 1996, **15**, 4264.
43 P. Belanzoni, N. Re, A. Sgamellotti and C. Floriani, *J. Chem. Soc.*, *Dalton Trans.*, 1997, 4773.
44 E. J. Baerends, D. E. Ellis and P. Ros, *Chem. Phys.*, 1973, **2**, 42; E. J. Baerends and P. Ros, *Chem. Phys.*, 1973, **2**, 51; E. J. Baerends and P. Ros, *Chem. Phys.*, 1975, **8**, 41; E. J. Baerends and P. Ros, *Int. J. Quantum. Chem.*, 1978, **S12**, 169.
45 P. M. Boerrigter, G. te Velde and E. J. Baerends, *Int. J. Quantum Chem.*, 1988, **33**, 87; G. Te Velde and E. J. Baerends, *J. Comput. Phys.*, 1992, **99**, 84.
46 T. Ziegler, V. Tschinke, E. J. Baerends, J. G. Snijders and W. Ravenek, *J. Phys. Chem.*, 1989, **93**, 3050.
47 S. H. Vosko, L. Wilk and M. Nusair, *Can. J. Phys.*, 1980, **58**, 1200.
48 A. D. Becke, *Phys. Rev.*, *Sect. A*, 1988, **38**, 2398.
49 J. P. Perdew, *Phys. Rev.*, *Sect. B*, 1986, **33**, 8822.
50 L. Noodleman and J. G. Norman, jun, *J. Chem. Phys.*, 1979, **70**, 4903.
51 K. J. Morokuma, *Chem. Phys.*, 1971, **55**, 1236; K. Kitaura and K. J. Morokuma, *Int. J. Quantum Chem.*, 1976, **10**, 325.
52 T. Ziegler and A. Rauk, *Theor. Chim. Acta*, 1977, **46**, 1.
53 J. Chatt, R. C. Fay and R. L. Richards, *J. Chem. Soc. A*, 1971, 2399; J. M. Treitel, M. T. Flood, R. E. March and H. B. Gray, *J. Am. Chem. Soc.*, 1969, **91**, 6512; D. Sellmann, *Angew. Chem.*, *Int. Ed. Engl.*, 1974, **13**, 639.
54 N. Re, M. Rosi, A. Sgamellotti, C. Floriani and E. Solari, *Inorg. Chem.*, 1994, **33**, 4390.
55 N. Re, M. Rosi, A. Sgamellotti and C. Floriani, *Inorg. Chem.*, 1995, **34**, 3410.
56 C. B. Powell and M. B. Hall, *Inorg. Chem.*, 1984, **23**, 4619.
57 M. R. A. Blomberg and P. E. M. Siegbahn, *J. Am. Chem. Soc.*, 1993, **115**, 6908.
58 I. S. Dmitriev, *Molecules Without Chemical Bonds*, Mir Publishers, Moscow, 1981.
59 I. Gutman and N. Trinajstic, *Top. Curr. Chem.*, 1973, **42**, 1.
60 M. D. Johnson, in *Comprehensive Organometallic Chemistry*, eds. G. Wilkinson, F. G. A. Stone and E. W. Abel, Pergamon Press, Oxford, 1982, vol. 4, p. 331.
61 A. M. Crespi and D. F. Shriver, *Organometallics*, 1985, **4**, 1830.
62 D. L. Lichtenberger, S. K. Renshow and R. M. Bullock, *J. Am. Chem. Soc.*, 1993, **115**, 3276; D. L. Lichtenberger, S. K. Renshow, R. M. Bullock, A. Wong and C. D. Tagge, *J. Am. Chem. Soc.*, 1993, **115**, 3276.
63 R. J. Lagow, J. J. Kampa, H. C. Wei, S. L. Battle, J. W. Genge, D. A. Laude, C. J. Harper, R. Bau, R. C. Stevens, J. F. Haw and E. Munson, *Science*, 1995, **267**, 362.
64 M. D. Ward, *Chem. Soc. Rev.*, 1995, 121.
65 C. Creutz, *Prog. Inorg. Chem.*, 1983, **30**, 1.
66 R. J. Crutchley, *Adv. Inorg. Chem.*, 1994, **41**, 273.
67 M. B. Robin and P. Day, *Adv. Inorg. Chem. Radiochem.*, 1967, **10**, 247.
68 G. Blondin and J. J. Girerd, *Chem. Rev.*, 1990, **90**, 1359.
69 A. A. Rashin and B. Honig, *J. Phys. Chem.*, 1985, **89**, 5588.
70 N. S. Hush, *Coord. Chem. Rev.*, 1985, **64**, 135; N. S. Hush, *Prog. Inorg. Chem.*, 1967, **8**, 391.
71 S. Woitellier, J. P. Launay and C. Joachim, *Chem. Phys.*, 1989, **89**, 481.

Received 28*th January* 1998; *Paper* 8/00770E